



Contents lists available at ScienceDirect

Journal of Quantitative Spectroscopy & Radiative Transfer

journal homepage: www.elsevier.com/locate/jqsrt

An evaluation of infrared microwindows for ozone retrievals using the Eureka Bruker 125HR Fourier transform spectrometer

Rodica Lindenmaier^{a,*}, Rebecca L. Batchelor^a, Kimberly Strong^a, Hans Fast^b, Florence Goutail^c, Felicia Kolonjari^a, C. Thomas McElroy^b, Richard L. Mittermeier^b, Kaley A. Walker^a

^a Department of Physics, University of Toronto, Toronto, ON, Canada M5S 1A7

^b Environment Canada, Toronto, ON, Canada M3H 5T4

^c Service d'Aéronomie, CNRS/IPSL, 91371 Verrieres le Buisson Cedex, France

ARTICLE INFO

Article history:

Received 22 July 2009

Received in revised form

15 October 2009

Accepted 17 October 2009

Keywords:

Ozone retrieval

Microwindow

Intercomparison

Infrared spectroscopy

CANDAC

PEARL

ABSTRACT

A Bruker 125HR Fourier transform spectrometer was installed at the Polar Environment Atmospheric Research Laboratory (PEARL) at Eureka, Nunavut, Canada in the summer of 2006 to study atmospheric composition. Using the optimal estimation method, typically over a limited spectral region called a microwindow, information about the vertical distribution of trace gas species that have absorption bands in the mid-infrared spectral range can be retrieved. Total and partial columns can also be determined to show the temporal evolution of the target gas. For ozone in particular, retrievals have been performed using several of its many mid-infrared absorption features, resulting in a lack of consistency in the literature in the microwindows chosen for retrievals. This work focuses on the optimization of the ozone retrieval, assessing a set of 22 microwindows between 780 and 3052 cm^{-1} to determine which is best suited to conditions at Eureka. The 1000–1004.5 cm^{-1} spectral interval is shown to be the most sensitive to both the stratosphere and troposphere. This microwindow gives the highest number of degrees of freedom for signal (~ 7 for total column), and the smallest total error (4.3%) compared with 21 other spectral regions. Retrievals performed with this microwindow agree well with results obtained from other instruments on-site. Total column ozone measured by the Bruker 125HR in this microwindow agreed to 2% with two other Fourier transform spectrometers, to 0.7% with a Brewer spectrophotometer, to 8% with a SAOZ UV–VIS spectrometer, and to 7% with ozone sondes.

© 2009 Elsevier Ltd. All rights reserved.

1. Introduction

Ozone is a naturally occurring substance which was first made in the laboratory in 1839 by Schönbein [1,2]. It is well known as an important component of our atmosphere, as it strongly absorbs solar ultraviolet (UV) radiation.

Total ozone column measurements in the first half of the twentieth century were mostly based on photometry in the UV wavelength range from 300 to 340 nm. Fabry and Buisson were the first to measure the atmospheric ozone column using a double spectrograph [3–5]. In the mid 1920s, Dobson designed the Fery spectrograph [6], which led to the development of the Dobson spectrophotometer which, in combination with its successor, the Brewer spectrophotometer [7], remains the backbone of the global ground-based ozone monitoring network today.

Many other techniques and instruments have since been developed to measure ozone concentrations. The

* Corresponding author. Tel.: +1 416 946 7129; fax: +1 416 978 8905.
E-mail address: rodica@atmosp.physics.utoronto.ca (R. Lindenmaier).

Table 1
Infrared microwindows previously used for ozone retrievals.

Reference	Spectral range (cm ⁻¹)	Interfering species (if available)
Vigouroux et al. [37], Senten et al. [38]	1000–1005	H ₂ O, CO ₂ , C ₂ H ₄ , O ₃ (668), O ₃ (686)
Wunch et al. [39], Taylor et al. [40]	3039.90–3040.60	H ₂ O, CH ₄
	2775.68–2776.30	CH ₄ , CO ₂ , HCl, N ₂ O
	2778.85–2779.20	CH ₄ , HDO, N ₂ O
	2781.57–2782.06	CH ₄ , HDO, N ₂ O, CO ₂
Yamamori et al. [41], Kagawa et al. [42]	3051.29–3051.90	H ₂ O, CH ₄ , HDO, CH ₃ D
Sung et al. [43], Fu et al. [30]	2775.78–2775.88	HCl, N ₂ O, CH ₄
	2775.68–2776.30	
	2778.90–2779.50	CH ₄ , CO ₂ , HCl, N ₂ O, HDO, solar lines
	2781.54–2782.09	
	1104.78–1105.08	CH ₃ D, CHF ₂ Cl, CCl ₂ F ₂ , H ₂ CO ₂ , HDO, O ₃ (668)
	1119.73–1119.95	CHF ₂ Cl, N ₂ O, O ₃ (668)
	1121.67–1122.03	O ₃ (668), H ₂ CO ₂ , CHF ₂ Cl, N ₂ O, H ₂ O
	1122.84–1123.06	O ₃ (668), H ₂ CO ₂ , CHF ₂ Cl, CH ₃ D, CH ₄ , H ₂ O
3039.80–3041.70	CH ₄ , H ₂ O, CH ₃ D	
Griesfeller et al. [44]	782.561–782.861	Not available
	788.850–789.369	
	1000.0–1005.0	
Hase et al. [45], Schneider et al. [35,18]	782.56–782.86	H ₂ O, CO ₂ , solar lines
	788.85–789.37	H ₂ O, CO ₂ , solar lines
	993.3–993.9	H ₂ O, CO ₂ , O ₃ (668), O ₃ (686)
	1000.0–1005.0	
	1007.3–1009.0	H ₂ O, CO ₂ , O ₃ —all isotopologs
	1011.1–1013.6	
Meier et al. [46]	3039.75–3040.55	CH ₄ , H ₂ O
	3045.08–3045.38	CH ₄
Barret et al. [17]	1002.567–1003.2	O ₃ (668), O ₃ (686)
	1000.0–1005.0	O ₃ (668), O ₃ (686), H ₂ O
Notholt et al. [47]	1002.58–1003.50	H ₂ O
	1003.90–1004.38	H ₂ O
	1004.58–1005.00	H ₂ O
Goldman et al. [48]	3045.08–3045.38	
	3027.42–3027.60	
Hamdouni et al. [16]	2107.80–2107.86	not available
	2780.81–2780.96	
	3037.32–3037.80	
Pougatchev et al. [20,15]	1002.567–1003.203	
Rinsland et al. [49]	764.03–764.43	
	773.20–773.38	
	781.08–781.25	CO ₂
	1127.60–1129.50	HDO, CH ₄
	1146.40–1146.56	
	1146.55–1147.40	N ₂ O, H ₂ O, HDO
	1155.39–1155.56	
	1162.85–1163.50	
	1163.34–1163.48	
	1167.50–1167.75	
	2083.50–2084.72	H ₂ O, CO ₂
	2754.55–2755.45	HDO, CH ₄ , solar lines
	2778.90–2779.20	
	2781.60–2781.86	HDO
	2792.65–2793.28	N ₂ O, HDO, solar
3040.00–3040.90	H ₂ O, CH ₄	
Adrian et al. [50], Wegner et al. [51]	996.5–998.5	H ₂ O, CO ₂
	2768.0–2773.0	HDO, H ₂ O, N ₂ O, CH ₄
	2773.0–2776.0	CH ₄ , N ₂ O, HDO, HCl

References are specified along with the spectral range used and the interfering species when they were available. The numbers in brackets for O₃ define its isotopes, with 6, 7, and 8 indicating ¹⁶O, ¹⁷O, and ¹⁸O, respectively.

first ozone measurements in the mid-infrared were made in the 1960s using a grating spectrometer flown on three balloon flights, which collected spectra for various altitudes from the ground through 30 km [8]. The first atmospheric measurements with Fourier transform spectrometers (FTSs) were performed at the Jet Propulsion Laboratory, Caltech [9]. The FTSs brought two important advantages compared to the grating spectrometers: the Fellgett advantage, i.e., all frequencies or wavelengths are measured simultaneously, and the Jacquinot advantage, i.e., high optical throughput that occurs because a circular aperture can be used [10]. Today, more than 20 high-resolution infrared FTSs regularly record atmospheric absorption spectra at sites distributed from pole to pole as part of the Network for the Detection of Atmospheric Composition Change (NDACC), which is committed to monitoring changes in the stratosphere, with an emphasis on the long-term evolution of the ozone layer [11].

FTSs operating in the mid-infrared are able to provide highly resolved solar absorption spectra from which precise total ozone column amounts can be retrieved. The high spectral resolution of the FTS measurements additionally allows vertical profile information to be determined from the pressure broadening of the absorption features. In practice, the vertical information content of a solar absorption spectrum is quantified by applying the optimal estimation method (OEM) of Rodgers [12–14]. This retrieved profile can then be used to determine total and partial columns. The sensitivity of the retrieval can be increased with a careful choice of the spectral region and with an appropriate selection of the absorption features.

The focus of this paper is the evaluation of ozone retrievals from mid-infrared measurements made with the new Bruker 125HR FTS installed at the Polar Environment Atmospheric Research Laboratory (PEARL) in Eureka, Nunavut, Canada (80.05°N, 86.42°W) in July 2006. Particular emphasis has been placed on the selection of the small spectral regions (known as microwindows) within which ozone is fitted. Many different microwindows containing ozone absorption features have been used by different groups for retrieval of ozone in the past. Until recently, narrow microwindows were used due to computational limitations, e.g., the 1002.6–1003.2 cm⁻¹ microwindow used by Pougatchev et al. [15] and the 2107.80–2107.86 cm⁻¹ microwindow used by Hamdouni et al. [16]. With recent advances in computational processing power, retrievals over broader microwindows encompassing multiple ozone absorption features have become possible. It has been demonstrated by Barret et al. [17] and Schneider et al. [18] that using broader microwindows increases the number of independent pieces of information in the retrieval, also called degrees of freedom for signal (DOFS).

Table 1 summarizes the mid-infrared ozone microwindows that have been used in ground-based Fourier transform infrared (FTIR) spectroscopy, demonstrating the lack of consistency in the literature. In the 2400–3100 cm⁻¹ region, one or more narrow microwindows are usually used. This is due to the high number of non-ozone absorption lines that affect the retrieval. The number of interfering species is much

smaller in the 600–1400 cm⁻¹ region, and therefore, the microwindows tend to be broader in this region.

In this study, spectral simulations were first performed for intervals of approximately 30 cm⁻¹ that contained strongly absorbing ozone lines and relatively few absorption lines due to interfering species. From these intervals, 22 smaller microwindows were then identified (as discussed in Section 3.1), overlapping with or extending the previously used ozone microwindows listed in Table 1. We evaluated these 22 microwindows to determine which is the most appropriate for ozone retrievals at our high Arctic site, identifying the spectral region that provides the highest DOFS and the smallest total error. The sensitivity of the retrieval to the stratosphere and troposphere for each microwindow was also investigated.

The paper is organized as follows. In Section 2, the instrument is briefly described along with our retrieval method. Section 3 presents the methodology used to define microwindows and assess their performance, and Section 4 contains the microwindow selection and error budget. Comparisons with other ozone-measuring instruments at Eureka for two periods (summer 2007 and spring 2008) are shown in Section 5. Section 6 concludes with a recommendation for the optimal microwindow for ozone retrievals with the Bruker 125HR FTS at Eureka.

2. Measurements

2.1. Instrumentation

In 2005, the Canadian Network for the Detection of Atmospheric Change (CANDAC) began operations at Eureka, establishing the Polar Environment Atmospheric Research Laboratory (PEARL). One of the key research themes at PEARL is to improve our understanding of the processes controlling the stratospheric ozone budget and its future evolution, using measurements of concentrations of a range of stratospheric constituents. To this end, a Bruker IFS 125HR FTS (referred to in this work as the Bruker 125HR) was installed in July 2006 and has since then been operated in the sunlit periods of the year since that time. In February 2009 it was certified as an NDACC instrument.

The Bruker 125HR is a scanning Michelson interferometer specifically designed for very high-resolution measurements over a broad spectral range. As weather permits, daily solar absorption measurements are performed using an automated measurement sequence stepping through a series of bandpass filters. Measurements are possible from approximately February 21 to October 20, when the sun is above the horizon. Spectra are normally recorded with boxcar apodization at a resolution of 0.0035 cm⁻¹, corresponding to a maximum optical path difference of 257 cm, using one of two detectors, indium antimonide (InSb) for the 1850–4400 cm⁻¹ region and mercury cadmium telluride (MCT) for the 600–1850 cm⁻¹ region, in combination with a potassium bromide (KBr) beamsplitter and a set of filters. For a detailed description of the instrument see Batchelor et al. [19].

2.2. The retrieval method

Retrievals of trace gas profiles from our Bruker 125HR spectra are performed using the OEM as described by Rodgers [12,13,14]. The retrieved profile ($\hat{\mathbf{x}}$) can be regarded as a linear combination of the *a priori* (\mathbf{x}_a) and the true (\mathbf{x}) profile with additional error contributions:

$$\hat{\mathbf{x}} = \mathbf{x}_a + \mathbf{A}(\mathbf{x} - \mathbf{x}_a) + \mathbf{G}_y \mathbf{K}_b (\mathbf{b} - \hat{\mathbf{b}}) + \mathbf{G}_y \boldsymbol{\varepsilon} \quad (1)$$

where \mathbf{A} represents the averaging kernel matrix, \mathbf{G}_y the gain matrix, \mathbf{K}_b the matrix showing the sensitivity of the forward model with respect to the forward model parameters \mathbf{b} , $\hat{\mathbf{b}}$ the estimated model parameters, and $\boldsymbol{\varepsilon}$ the measurement error. The OEM requires the *a priori* volume mixing ratio (VMR) profile of the target gas, the associated *a priori* covariance matrix and the *a priori* VMR profiles of the interfering species. The retrieved state vector contains the VMR of the target gas on discrete layers in the atmosphere, and all other fitted parameters for the interfering species and model parameters. The vertical information content of the retrieved profile can be optimized with a good choice of microwindow(s) and *a priori* information.

The retrieval algorithm used to analyze the Bruker spectra was SFIT2 v3.92c, a radiative transfer and profile retrieval algorithm based on the OEM. A calculated spectrum is fitted to the observed one by means of adjustment of the gas profiles and supplementary instrumental parameters [15,20,21]. The SFIT2 algorithm permits retrievals using one or more microwindows. The forward model of SFIT2 is “a multi-layer, multi-species, line-by-line transfer model which was developed for the analysis of FTIR spectra” [15]. The model assumes that the layers are homogeneous and in local thermodynamic equilibrium, and it also assumes a Voigt line shape function, refractive ray-tracing calculations using the *fscatm* algorithm [22], site-specific pressure and temperature profiles, and instrument line shape (ILS) function calculations (including the effects of apodization, maximum optical path difference (MOPD), and finite field-of-view).

fscatm was used to convert the pressure, temperature and VMR profiles specified at 63 layer boundaries to density-weighted effective pressure, temperature and VMR profiles within the 38 layers that form the vertical retrieval grid used at Eureka [19]. The pressure and temperature profiles were obtained from the mean of the two radiosondes launched daily at Eureka by Environment Canada. This information was supplemented with the National Centre for Environmental Prediction (NCEP) profiles above the maximum heights of the radiosondes, and with the 1976 US standard atmosphere profile above 50 km [19]. The *a priori* ozone profile was developed by Sung (personal communication). For the altitude range of 0.6–35 km, the average of 13 years (1993–2005) of ozone sonde measurements at Eureka for the sunlit February–September period was used. Averaged HALOE ozone data from the same months were used above 35 km [23]. The updated HITRAN 2004 database was used for line-by-line calculations of the atmospheric spectrum [24].

The *a priori* covariance matrix \mathbf{S}_a , which constrains the retrieval to the *a priori*, was set to 70% uncertainty on the diagonal with a Gaussian 4 km interlayer correlation from 0.6 to 100 km. The 70% uncertainty represents the maximum variability in ozone observed in the Eureka ozone sonde data record (1σ on the 13-year mean). For the interfering species, the *a priori* diagonal covariances were set to 100% with no interlayer correlation.

The optimal value of the signal-to-noise ratio (SNR) as a fitting parameter, used to determine the retrieval noise covariance matrix, was chosen after constructing the trade-off curves of the root mean square (RMS) fitting residual as a function of SNR for each microwindow. For a description of this technique see Batchelor et al. [19].

3. Methodology

3.1. Microwindows

A series of ozone microwindows found in the NDACC filter 6 (600–1400 cm^{-1}) and filter 3 (2400–3100 cm^{-1}) regions, on the MCT and InSb detectors respectively, were investigated. Simulations were used to identify the interfering species for each spectral interval. The *a priori* VMR profiles and the pressure and temperature profiles used in the simulations were the same as those used in the retrievals (discussed in Section 2.2). The absorptions for ozone and the interfering species and their mean values were calculated for each interval of interest. This helped in the selection of the regions where the ozone lines were strong enough for retrieval and minimally influenced by interfering species. It also identified the key interfering species that should be included in each retrieval.

After the initial definition of the spectral regions of interest, preliminary retrievals were performed and the RMS fitting residuals were examined for systematic features indicative of issues with the spectroscopic parameters in the HITRAN database. These results were used to refine the choice of microwindows. In total, 22 microwindows and multi-microwindows (meaning that more than one microwindow is fitted simultaneously) were chosen in our study for further analysis and are presented in Table 2, along with the values of the SNR determined from the trade-off curves for each microwindow combination and the interfering species included in each case. The microwindow designation for each microwindow combination, as listed in column two, approximates the spectral region, with the letter “m” identifying a multi-microwindow fit.

3.2. Averaging kernels

The combined forward model and retrieval system with respect to the true atmosphere is characterized by the averaging kernel matrix, \mathbf{A} . The rows of this matrix are the averaging kernels (or smoothing functions), which describe what proportion of each of the altitude layers in the true profile is represented in the determination of that retrieved altitude layer [14]. Summing the elements of

Table 2

List of ozone microwindows examined in this work, their designation and spectral range, the SNR used in the retrieval, and the interfering species included in the retrievals.

	Microwindow designation	Spectral range (cm ⁻¹)	SNR	Interfering species
1	782	780.70–783.10	100	CO ₂ , H ₂ O, HNO ₃ , ClONO ₂ , C ₂ H ₂ , CCl ₄ , COF ₂ , C ₂ H ₆ , HCN, solar
2	984	785.55–790.30		CO ₂ , H ₂ O, HNO ₃ , ClONO ₂ , C ₂ H ₂ , CCl ₄ , C ₂ H ₆ , HCN, solar
3	984 m	984.47–985.28	100	O ₃ (686), CO ₂ , O ₃ (668), H ₂ O, C ₂ H ₄
		986.10–988.09	100	O ₃ (686), CO ₂ , O ₃ (668)
		988.30–990.00		O ₃ (686), O ₃ (668), CO ₂ , C ₂ H ₄
4	987	986.10–988.10	100	O ₃ (686), O ₃ (668), CO ₂ , H ₂ O, C ₂ H ₄
5	988	988.70–990.00	100	O ₃ (686), CO ₂ , O ₃ (668), C ₂ H ₄
6	1000	1000.00–1004.5	100	O ₃ (686), CO ₂ , O ₃ (668)
7	1088	1000.00–1004.5	100	H ₂ O, CO ₂ , O ₃ (676), O ₃ (667), O ₃ (686), O ₃ (668), C ₂ H ₄
8	1090	1088.10–1091.00	100	CO ₂ , H ₂ O, O ₃ (668), CCl ₃ F, CCl ₂ F ₂ , HCOOH, CHF ₂ Cl
9	1106	1085.70–1091.00	100	CO ₂ , H ₂ O, O ₃ (668), CCl ₃ F, CCl ₂ F ₂ , HCOOH, CHF ₂ Cl
10	1119	1101.70–1106.50	100	CO ₂ , H ₂ O, O ₃ (668), CCl ₃ F, CHF ₂ Cl, HDO, HCOOH, O ₃ (668)
11	1119 m	1112.00–1117.40	100	H ₂ O, CCl ₂ F ₂ , CH ₃ D, CHF ₂ Cl, HDO, HCOOH, O ₃ (668)
		1112.00–1117.40	100	H ₂ O, CCl ₂ F ₂ , CH ₃ D, CHF ₂ Cl, HDO, HCOOH, O ₃ (668)
		1118.85–1120.50		N ₂ O, H ₂ O, CCl ₂ F ₂ , CH ₃ D, CHF ₂ Cl, SO ₂ , HDO, HCOOH
12	1123	1123.85–1133.92	100	N ₂ O, H ₂ O, CCl ₂ F ₂ , CH ₃ D, CHF ₂ Cl, SO ₂ , HDO, HCOOH, solar
13	1146 m	1138.00–1140.85	100	N ₂ O, H ₂ O, CCl ₂ F ₂ , CH ₃ D, CHF ₂ Cl, SO ₂ , HDO, CH ₄
		1142.65–1148.80		N ₂ O, H ₂ O, CCl ₂ F ₂ , CH ₃ D, CHF ₂ Cl, SO ₂ , HDO, CH ₄
14	1148	1142.65–1148.80	100	N ₂ O, H ₂ O, CCl ₂ F ₂ , CH ₃ D, CHF ₂ Cl, SO ₂ , HDO, CH ₄
15	1170	1175.80–1180.50	100	CH ₄ , H ₂ O, CCl ₂ F ₂ , CH ₃ D, SO ₂ , HDO, N ₂ O, HNO ₃ , HCFC-142b
16	2775	2766.50–2775.50	200	CH ₄ , N ₂ O, CO ₂ , H ₂ O, HDO, HCl, solar
17	3023	3023.35–3023.85	200	H ₂ O, CH ₄ , CH ₃ D, CH ₃ Cl, C ₂ H ₄
18	3023 m	3023.70–3024.07	170	H ₂ O, CH ₄ , CH ₃ D, CH ₃ Cl, C ₂ H ₄
		3039.75–3040.55		H ₂ O, CH ₄ , CH ₃ D, CH ₃ Cl, C ₂ H ₄
		3045.09–3040.65		H ₂ O, CH ₄ , CH ₃ D, CH ₃ Cl, HDO, C ₂ H ₄
19	3040 m	3023.40–3023.55	170	H ₂ O, CH ₄ , CH ₃ D, CH ₃ Cl, C ₂ H ₄ , N ₂ O, solar
		3040.90–3041.01		CH ₄ , H ₂ O, CH ₃ D, CH ₃ Cl, HDO, N ₂ O, C ₂ H ₄ , solar
		3042.85–3043.16		H ₂ O, CH ₄ , CH ₃ D, CH ₃ Cl, HDO, HCl, solar
		3044.25–3044.50		H ₂ O, CH ₄ , CH ₃ D, CH ₃ Cl, HDO, HCl, solar
20	3041	3039.91–3042.20	170	H ₂ O, CH ₄ , CH ₃ D, CH ₃ Cl, solar
21	3045	3044.20–3045.74	170	CH ₄ , H ₂ O, CH ₃ D, CH ₃ Cl, HDO, N ₂ O, C ₂ H ₄ , solar
22	3051 m	3051.35–3051.52	150	CH ₄ , H ₂ O, CH ₃ D, HDO, solar
		3051.77–3051.88		CH ₄ , H ₂ O, CH ₃ D, HDO, solar

The microwindow designation for each microwindow combination, as listed in column two, approximates the spectral region, with the letter “m” identifying a multi-microwindow fit. The numbers in brackets for O₃ define its isotopes, with 6, 7, and 8 indicating ¹⁶O, ¹⁷O, and ¹⁸O, respectively.

each row determines the area under the averaging kernel (also called sensitivity), which is indicative of the fraction of the retrieval that comes from the measurement rather than from the *a priori*. Total or partial column averaging kernels are determined by weighting the averaging kernel information for each layer by the ozone density profile, and summing over the altitude range of interest. The number of independent pieces of information contained in the measurement is called degrees of freedom for signal, DOFS. In this work the trace of the averaging kernel matrix, $\text{tr}(\mathbf{A})$, is used to determine the DOFS [14]. The averaging kernels and DOFS have been used to assess the vertical information content of the retrievals for each microwindow, thereby identifying the microwindow(s) having the highest information content.

3.3. Error analysis

The error calculations in this work are based on the methodology of Rodgers [14]. In addition to the smoothing (\mathbf{S}_s) and measurement (\mathbf{S}_m) errors, forward model parameter errors have been calculated using a perturbation method and our best estimate of the uncertainties in temperature (\mathbf{S}_{temp}), line intensity (\mathbf{S}_{lint}), air-broadened half width ($\mathbf{S}_{\text{lwidth}}$), and solar zenith angle (\mathbf{S}_{sza}) have also

been included. Interference errors, as described by Rodgers and Connor [25] have been calculated to account for uncertainties in retrieval parameters (i.e., wavelength shift, instrument line shape, background slope and curvature, and phase error) and in interfering gases simultaneously retrieved. These interference errors are referred to as \mathbf{S}_{int1} and \mathbf{S}_{int2} , respectively. The error budget calculation is described in depth by Batchelor et al. [19].

The total error ($\mathbf{S}_{\text{TOTAL}}$) has been determined by adding all components in quadrature and not taking into account differences between the random and systematic components:

$$\mathbf{S}_{\text{TOTAL}} = \{(\mathbf{S}_m^2 + \mathbf{S}_{\text{temp}}^2 + \mathbf{S}_{\text{int1}}^2 + \mathbf{S}_{\text{int2}}^2 + \mathbf{S}_{\text{sza}}^2) + \mathbf{S}_{\text{lint}}^2 + \mathbf{S}_{\text{lwidth}}^2 + \mathbf{S}_s^2\}^{1/2} \quad (2)$$

In many cases, however, it is useful to exclude the smoothing error (because this can be accounted for when doing comparisons) and the spectroscopic line parameters (because these are truly systematic), and as such, we define the total random error (\mathbf{S}_{totr}) as the sum of the measurement error, interference errors, and errors due to uncertainties in solar zenith angle and temperature, added in quadrature (represented by the sum within the round brackets in Eq. (2)).

4. Results and discussion

4.1. Comparison of microwindows

Retrievals were performed using spectra recorded during August 2007 and March 2008 using each of the 22 microwindows listed in Table 2. Fig. 1 shows typical fits for a selection of 12 of these microwindows. It is evident that the number and depth of the absorption lines is very different from one microwindow to the other (e.g., 782 compared to 1123). Systematic features in the residual tend to correspond to poor spectral parameters in the HITRAN database, often corresponding to CH₄ features. These have been avoided in many cases by removing badly affected regions. In the case of microwindow 3041, the simultaneous retrieval of O₃ with CH₄ could not remove the spikes in the residual, corresponding to CH₄ spectral lines. These residuals may also in part be due to the use of the Voigt line shape in the forward model. Use of a line shape model that accounts for line-mixing effects can significantly improve the fitting residuals for some spectra [26]. This has not, however, been investigated in this work. For microwindow 3051 m, two narrow microwindows were used in order to exclude regions having similar spikes (not shown in Fig. 1). Most of the microwindows in the filter 3 region are dominated by interfering species, making it difficult to obtain good retrievals, as seen from the larger fitting residuals.

The vertical sensitivity of each microwindow was examined using the VMR averaging kernels, which are shown in Fig. 2 for 20 of the 22 microwindows, e.g., microwindows 3023, 3041, 3045, and 3051 m display almost no sensitivity in the troposphere, while 984 m, 1000, and 1123 are sensitive in this region.

The filter 6 spectral interval is more suitable for broad microwindows as the number of strongly interfering species is smaller. As a result of having fewer interfering species, we can additionally fit minor species with very small interference, resulting in better retrievals and smaller residuals. Examples of microwindows with high total column DOFS and high tropospheric sensitivity are 1000, 1119, 1123, and 1146 m. The DOFS for the microwindows in the filter 6 spectral region are, in general, higher by at least 1, sometimes by 2 or 3, compared to the DOFS for microwindows in the filter 3 spectral region. This is explained by the larger number of lines and greater range of intensities in the filter 6 region, which allows us to probe different altitudes of the atmosphere.

Fig. 3 presents the 0.6–8 km partial column (dotted lines), 8–50 km partial column (dashed lines), and the total column (solid lines) averaging kernels. Most of the filter 6 microwindows are seen to have significant tropospheric column averaging kernels, while the filter 3 microwindows have much smaller tropospheric column averaging kernels, as seen for example for 3051 m. The stratospheric column averaging kernels show only small differences for each microwindow, and are close to 1 between 8 and 50 km in all cases.

Scatter plots of columns retrieved in pairs of microwindows were constructed to assess the correlations of the tropospheric, stratospheric, and total columns. All

spectra recorded from March 1 to April 8, 2008, corresponding to the Canadian Arctic ACE Validation Campaign (to be discussed in Section 5) were used. Pairs of measurements were considered matched if they were made within 1 h of each other. Results are shown for microwindow 1000 versus 1123, 3023 m, and 3051 m, where microwindows 1000 and 1123 are sensitive in both the tropospheric and stratospheric regions, while 3023 m is less sensitive in the troposphere and 3051 m is only sensitive in the stratosphere. The top row of Fig. 4 (panels a–c) shows the scatter plots and linear fits for the stratospheric partial columns, 8–50 km. In general, for the stratosphere, there is a good correlation for each pair, with the correlation coefficient (*R*) and slope (*S*) being very close to 1, and the intercept (*I*) being very small. While there is good correlation in all three cases, it is marginally better for the 1000 and 1123 pair than for the 1000 and 3023 m or 3051 m pairs, as expected by the sensitivity shown in Fig. 3.

The middle row of Fig. 4 (panels d–f) shows similar plots for the tropospheric partial columns, 0.6–8 km. As expected from the sensitivity plots, the tropospheric information is more varied from microwindow to microwindow. For the first pair of microwindows, 1000 versus 1123, both of which contain information in the troposphere, the agreement is good. For the latter two pairs of microwindows, the correlations are not so good, as expected.

For the total columns from 0.6 to 100 km, the correlations are given in the bottom row of Fig. 4 (panels g–i). These plots are very similar to those for the stratosphere, with excellent correlations. The slope of 0.92 in (i) versus 1.01 for the stratospheric partial columns (c) for the 1000 versus 3051 m pair can be attributed to the differences in the total column averaging kernels for microwindow 1000 versus 3051 m (shown in Fig. 3). The total column plots show that the choice of microwindow(s) is less critical if the measurement of interest is total column ozone than if vertical information is of interest. This is highlighted in Fig. 5, which shows the percentage difference between the columns retrieved for each of these microwindows with respect to microwindow 1000, along with the mean and standard deviation. The percentage difference between the total columns is given by

$$\%Diff = 100\% * [(MW1000 - MWx)/(MW1000 + MWx) * 0.5] \quad (3)$$

where *MW1000* represents the total column retrieved using microwindow 1000 and *MWx* represents the total column using one of the other previously mentioned microwindows. The mean differences for microwindow 1000 versus 1123 and 3023 m (Fig. 5, panels a and b) are less than 1%, indicating that the retrieved columns are almost identical. For the 1000 versus 3051 m pair (panel c), the percentage difference is larger than in the previous two cases, at –6.17%. The scatter, represented by the standard deviation, is also greater for this microwindow pair, suggesting that the 3051 m retrievals are not as consistent as the other microwindows. A list of mean differences for the ozone total columns and their standard

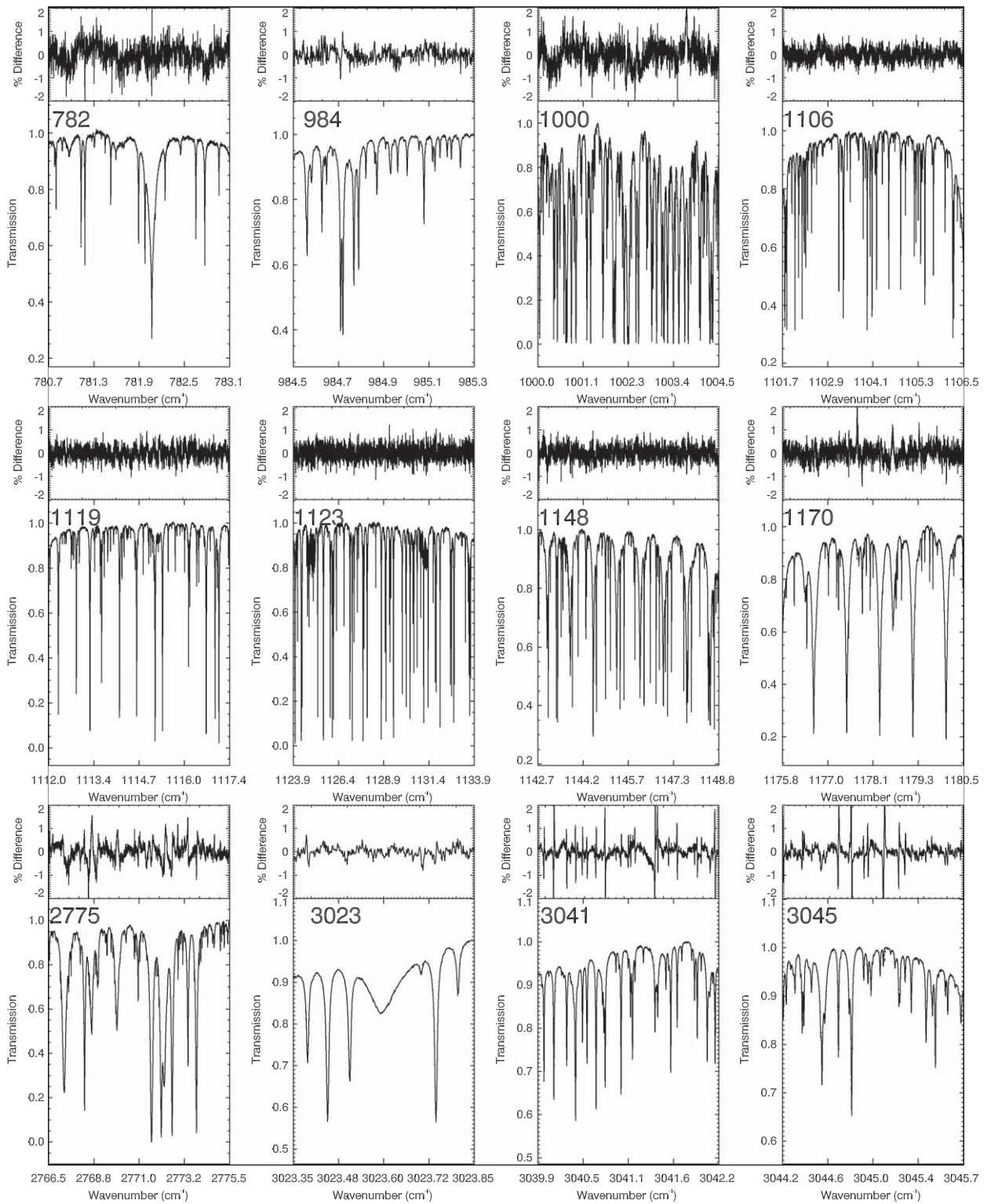


Fig. 1. Examples of fits and residuals for 12 of the 22 ozone microwindows studied. The spectra were recorded on August 30, 2007. The measured spectra are indicated by the solid line, and the calculated spectra are indicated by the dashed line (generally not visible). The residuals are calculated as the difference between the measured and calculated spectra.

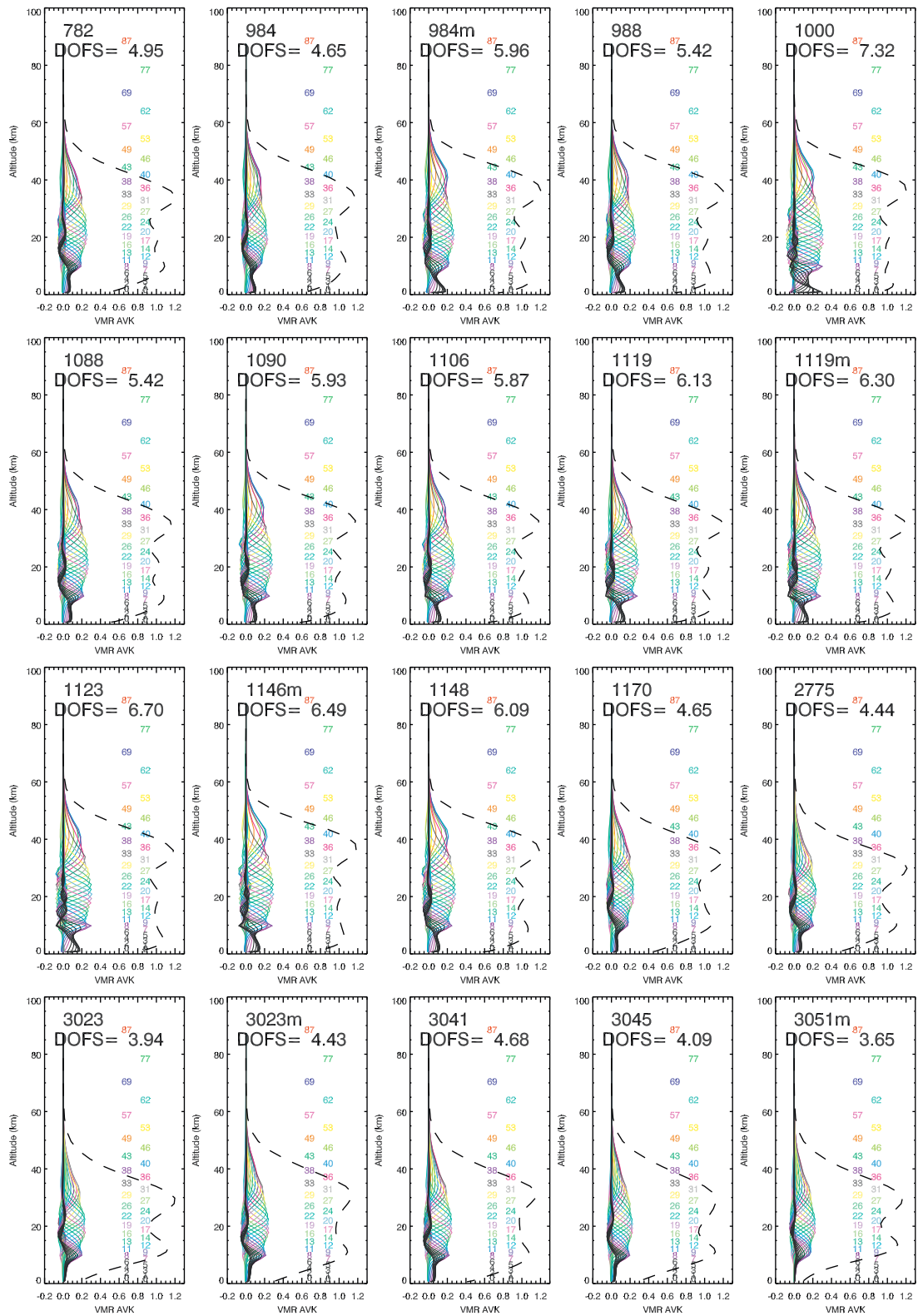


Fig. 2. Ozone VMR averaging kernels for spectra recorded on August 30, 2007 for 20 of the 22 microwindows studied. Each color corresponds to one of the 38 retrieved layers, with the altitude of each layer in km indicated on the right of each panel. The dashed line shows the sensitivity of the retrieval to the measurement. The DOFS is given for each microwindow.

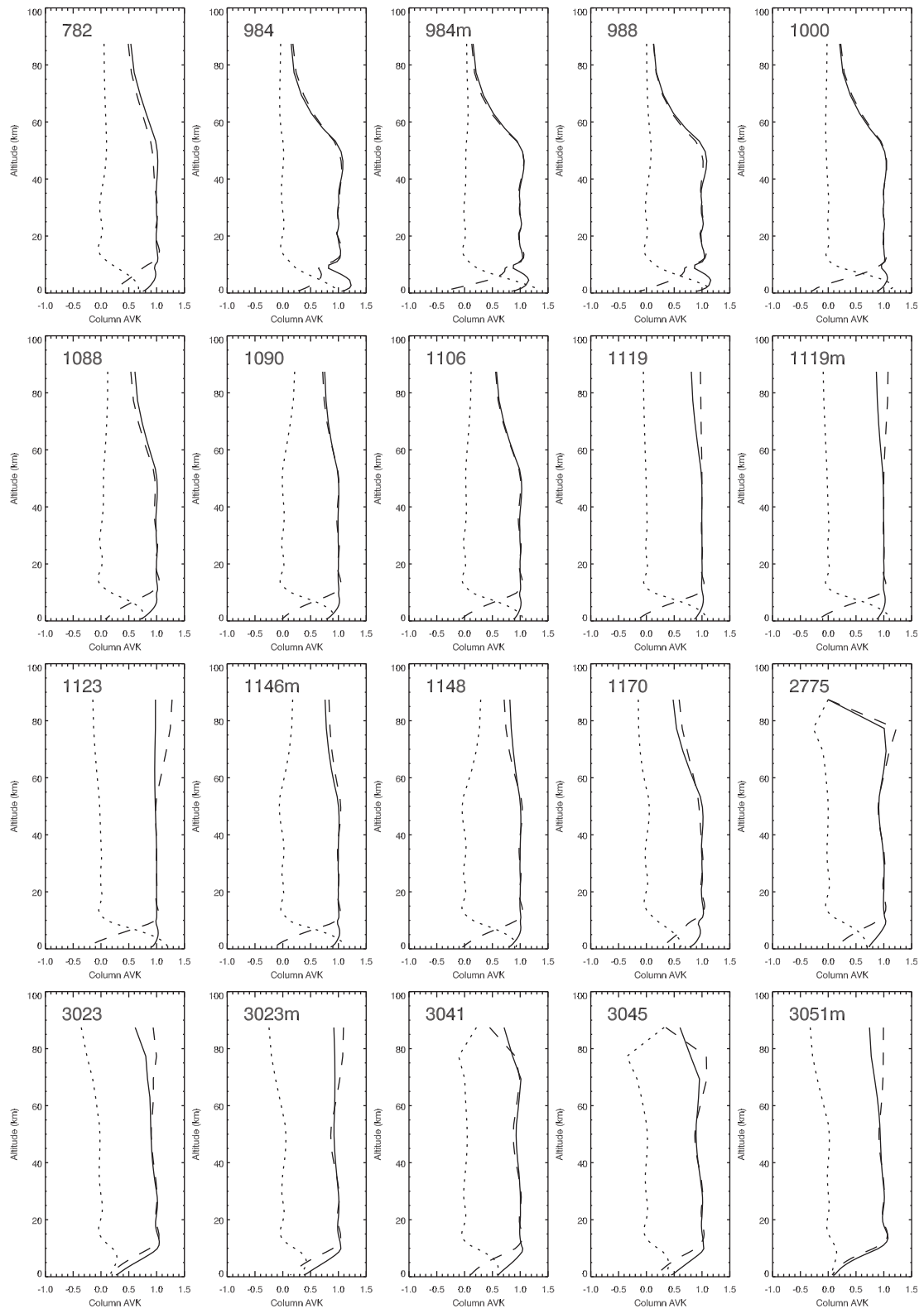


Fig. 3. Ozone column averaging kernels for spectra recorded on August 30, 2007 for 20 of the 22 microwindows studied. The solid line indicates the total column (0.6–100 km) averaging kernel. The dotted line corresponds to the tropospheric partial column (0.6–8 km) and the dashed line to the stratospheric partial column (8–50 km).

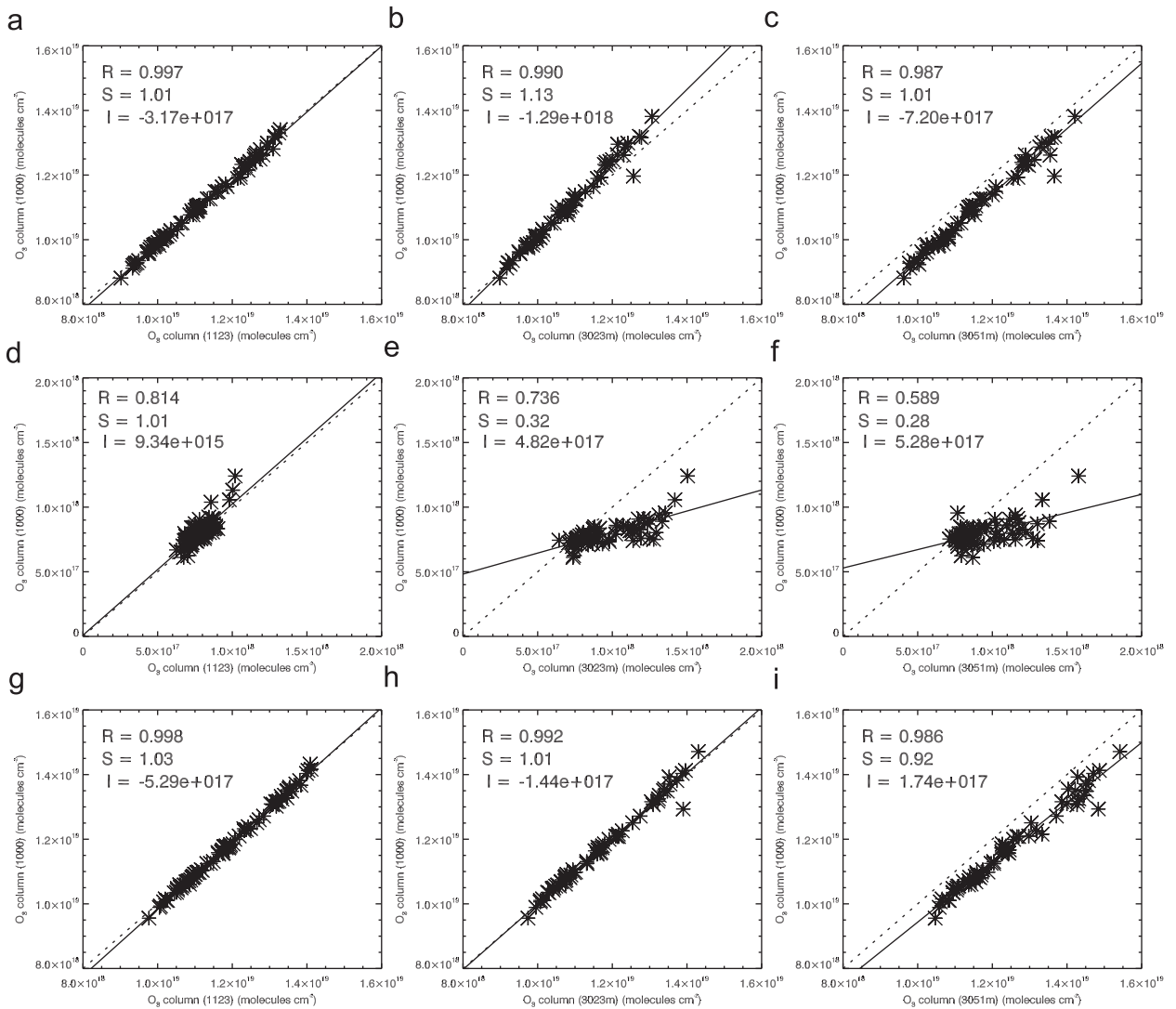


Fig. 4. Top row: scatter plots for pairs of microwindows for the stratospheric ozone partial columns (8–50 km). (a) Microwindow 1000 versus 1123, (b) 1000 versus 3023 m and (c) 1000 versus 3051 m. Middle row: same as above but for the tropospheric ozone partial column (0.6–8 km). The spectra were recorded in spring 2008 (March 1–April 8). The correlation coefficient (R), slope (S) and intercept (I) are given for each comparison. The solid black line shows the best fit for the comparison, and the dotted line shows the 1:1 line.

deviations for microwindow 1000 versus each of the other 21 microwindows is given in Table 3.

4.2. Error budget

Table 4 provides the error budget for the ozone total column calculated as discussed in Section 3.3, for all 22 of the microwindows studied. For the filter 6 region, a spectrum recorded on August 30, 2007 at 10:20:55 local time (LT) at a solar zenith angle (SZA) of 73.07° was used. For the filter 3 region, a spectrum recorded on the same day at 11:21:42 LT, at a SZA of 71.78° was used. The choice of these spectra was based on the fact that August 30 was a very clear day, optimal for FTS measurements.

Measurement errors (S_m) vary from 0.23% for microwindow 1000 to 3.48% for 3051 m and are generally

higher for the filter 3 microwindows. Microwindows 984, 984 m, 987, 988, and 3040 m, have the largest uncertainties (approx. 2 to 2.5%) due to temperature (S_{temp}), while 1088, 1090, 1106 and 1146 m have the smallest values ($\leq 0.20\%$). The uncertainties due to the retrieved instrument parameters (S_{int1}) and the retrieved interfering species (S_{int2}) are higher in the filter 3 region, as expected from the narrower microwindows and the larger interference of other gases. The uncertainties resulting from changes in the SZA (S_{sza}) are very similar for all the microwindows, as expected from the identical time required for each measurement. The uncertainties coming from the spectroscopic parameters (S_{fint} and S_{width}) have similar values across the microwindows, however microwindow 1000 has less than half the uncertainty of the other microwindows for the line intensity (4.24%), but a larger uncertainty for the line width compared to the

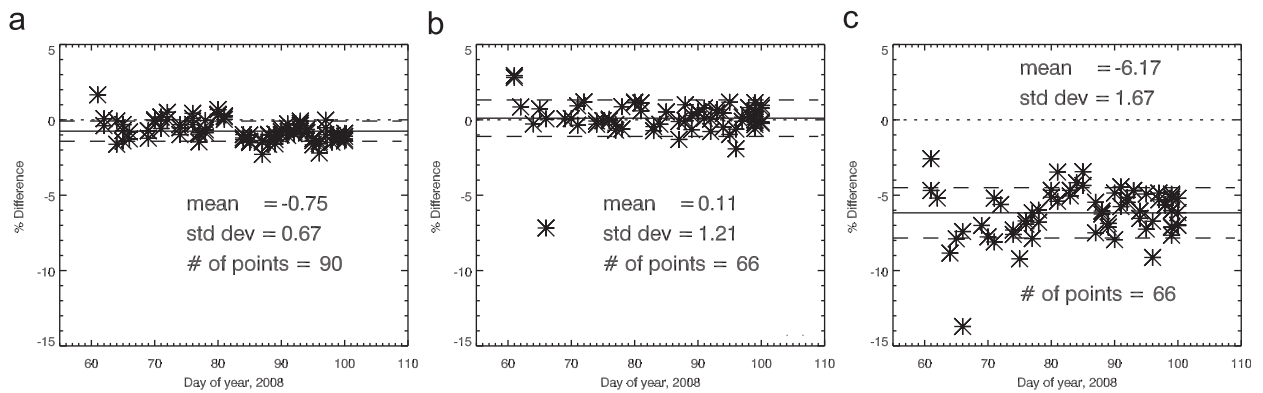


Fig. 5. Percentage differences for the ozone total columns for microwindow 1000 versus (a) 1123, (b) 3023 m, and (c) 3051 m. The percentage difference is calculated using Equation (3). The mean percentage difference (solid line), standard deviation (dashed lines), and number of points compared are given for each case. The dotted line shows the zero difference.

Table 3

Mean differences in the ozone total columns and their standard deviations (both in %), for the 1000 microwindow compared with each of the other 21 microwindows, for spring 2008.

Microwindow designation	Mean difference (%)	Standard deviation (%)
782	2.04	1.39
984	0.27	1.04
984 m	0.96	0.82
987	1.35	0.75
988	0.44	0.73
1088	-0.41	1.07
1090	-0.44	1.02
1106	0.27	1.22
1119	-0.23	1.06
1119 m	-0.44	0.99
1123	0.75	0.67
1146 m	0.36	0.82
1148	0.32	0.95
1170	-0.16	1.17
2775	6.16	2.15
3023	0.23	1.88
3023 m	0.11	1.21
3040 m	-1.58	1.97
3041	3.11	1.85
3045	-4.03	1.50
3051 m	-6.17	1.67

The number of compared spectra was 90 for the filter 6 microwindows and 66 for the filter 3 microwindows.

other filter 6 microwindows (0.4%). The line width difference could be due to saturation effects, since this microwindow contains the largest number of lines with nearly 100% absorption compared to the other microwindows.

The total error column clearly shows that microwindow 1000 has the smallest uncertainty of the 22 microwindows (4.34%). This microwindow also has the largest information content as shown by the DOFS in the last column (7.32). Similar results are shown in Tables 5 and 6, which give the error budgets calculated for the spectra mentioned above, for the stratospheric (8–50 km) and tropospheric (0.6–8 km) columns, respec-

tively. As for the total column calculations, microwindow 1000 is seen to have the highest DOFS and lowest errors for both partial columns.

Similar calculations (not shown) have been performed for spectra recorded during spring 2008, when the sun is lower and the instrument consequently looks through more atmosphere. In all cases, the relative results for the microwindows were similar, but the DOFS were higher and the total errors smaller (e.g., 7.58% and 1.52% for the total column using microwindow 1000), reflecting the additional information contained in the deeper absorption features.

Combining the information gained from the averaging kernels, column scatter plots and error analysis, it is clear that the 1000 microwindow, covering the broad spectral range 1000 to 1004.5 cm^{-1} is the best choice for ozone retrievals using the Bruker 125HR at Eureka.

5. Comparison with other instruments

Since 2004, there has been an annual springtime Canadian Arctic Atmospheric Chemistry Experiment (ACE) validation campaign at Eureka (e.g., [27]). During this time, intensive ozone measurements are made with a variety of instruments, including FTs, ultraviolet–visible (UV–VIS) spectrometers, Brewer spectrophotometers, and ozone sondes. During the 2008 campaign, three FTs measured side-by-side, sharing the same solar beam [28]. These included the Bruker 125HR, the Bomem DA8 FTS [29] and the Portable Atmospheric Research Interferometric Spectrometer for the Infrared (PARIS-IR) [30]. In addition, two UV–VIS instruments, Brewer spectrophotometer #21 [31], located at the Eureka Weather Station, and the SAOZ (Système d’Analyse par Observation Zénithale) [32] were in operation.

Fig. 6 shows the ozone total column time series measured with each of these instruments during the campaign. In addition, total column ozone determined from regularly launched ozone sondes and from profiles recorded with the ACE-FTS [33] onboard the SCISAT satellite are shown. For ozone sondes, the total column

Table 4

The error budget for ozone total column (0.6–100 km) for August 30, 2007: SZA=73° for the filter 6 (600–1400 cm⁻¹) region, SZA=72° for the filter 3 (2400–3100 cm⁻¹) region.

MW	S _m (%)	S _{temp} (%)	S _{int1} (%)	S _{int2} (%)	S _{sza} (%)	S _{totr} (%)	S _{lint} (%)	S _{lwidth} (%)	S _s (%)	S _{TOTAL} (%)	DOFS
782	1.42	1.40	0.03	0.18	0.80	2.16	12.37	0.11	0.56	12.57	4.95
984	1.70	2.53	0.39	0.09	0.68	3.15	10.15	0.12	1.48	10.73	4.65
984 m	0.72	1.96	0.05	0.08	0.61	2.17	9.14	0.10	0.97	9.45	5.97
987	0.96	2.03	0.03	0.06	0.60	2.32	9.09	0.09	1.15	9.45	5.47
988	0.89	2.13	0.09	0.004	0.61	2.39	9.10	0.10	1.08	9.47	5.43
1000	0.23	0.69	0.01	0.003	0.27	0.77	4.24	0.40	0.33	4.34	7.32
1088	1.17	0.09	0.31	0.25	0.71	1.43	11.04	0.05	0.33	11.14	5.42
1090	0.83	0.10	0.17	0.15	0.69	1.10	10.82	0.05	0.21	10.88	5.94
1106	0.70	0.13	0.21	0.02	0.75	1.06	11.42	0.02	0.20	11.47	5.87
1119	0.61	0.58	0.09	0.04	0.79	1.16	11.76	0.12	0.27	11.82	6.14
1119 m	0.54	0.63	0.07	0.03	0.78	1.14	11.65	0.13	0.25	11.71	6.31
1123	0.30	0.41	0.04	0.01	0.74	0.89	11.03	0.17	0.13	11.06	6.71
1146 m	0.64	0.20	0.08	0.05	0.70	0.98	10.98	0.04	0.21	11.03	6.50
1148	0.93	0.34	0.09	0.09	0.69	1.22	10.87	0.05	0.39	10.95	6.09
1170	1.76	0.65	0.20	0.18	0.64	1.10	11.10	0.14	0.65	11.29	4.65
2775	1.15	1.28	0.01	0.35	0.50	1.83	11.53	0.24	0.29	11.68	4.45
3023	2.68	0.95	1.78	0.23	0.65	3.43	10.54	0.59	2.30	11.34	3.95
3023 m	2.08	1.24	1.50	0.24	0.77	2.96	12.46	0.60	1.78	12.94	4.44
3040 m	3.40	2.11	2.72	2.57	0.73	5.53	12.58	1.48	1.24	13.88	3.73
3041	1.53	1.19	0.38	0.79	0.71	2.24	11.54	0.07	0.40	11.77	4.69
3045	2.27	1.61	0.38	0.42	0.71	2.93	11.81	0.65	1.50	12.27	4.10
3051 m	3.48	1.00	3.72	0.81	0.62	5.30	10.15	1.16	3.60	12.06	3.65

The covariance matrices are defined in the text.

Table 5

The error budget for stratospheric ozone partial column (8–50 km), for the same spectra as in Table 4.

MW	S _m (%)	S _{temp} (%)	S _{int1} (%)	S _{int2} (%)	S _{sza} (%)	S _{totr} (%)	S _{lint} (%)	S _{lwidth} (%)	S _s (%)	S _{TOTAL} (%)	DOFS
782	1.79	0.19	0.04	0.12	0.87	2.01	13.29	0.61	2.70	13.72	4.44
984	2.74	2.55	0.43	0.17	0.67	3.83	10.01	0.45	3.72	11.35	4.01
984 m	1.52	1.58	0.08	0.11	0.54	2.26	8.23	0.61	2.30	8.86	4.95
987	1.95	1.92	0.04	0.12	0.56	2.79	8.48	0.61	2.65	9.33	4.55
988	1.93	1.67	0.10	0.02	0.55	2.61	8.32	0.50	2.68	9.14	4.58
1000	0.55	0.52	0.03	0.02	0.22	0.79	3.36	0.90	1.29	3.79	5.86
1088	1.42	1.02	0.39	0.19	0.74	1.95	11.52	0.56	1.50	11.79	4.80
1090	1.28	1.74	0.32	0.15	0.73	2.31	11.46	0.66	1.32	11.78	5.18
1106	1.34	1.70	0.46	0.03	0.78	2.35	12.06	0.74	1.54	12.41	5.04
1119	0.94	1.70	0.14	0.03	0.80	2.11	12.00	1.00	1.23	12.29	5.22
1119 m	0.84	1.70	0.09	0.02	0.80	2.06	11.92	1.03	1.18	12.20	5.36
1123	0.68	1.85	0.04	0.02	0.77	2.12	11.58	1.04	1.14	11.87	5.63
1146 m	1.07	2.36	0.24	0.07	0.70	2.69	10.95	0.50	1.22	11.36	5.57
1148	1.25	1.56	0.26	0.12	0.68	2.14	10.94	0.50	1.58	11.26	5.33
1170	1.94	0.29	0.07	0.16	0.66	2.08	11.43	0.53	2.73	11.94	4.19
2775	1.48	1.39	0.12	0.19	0.71	2.17	12.38	1.41	1.08	12.69	3.91
3023	2.03	1.27	1.74	0.12	0.68	3.04	11.30	1.21	2.21	11.98	3.76
3023 m	1.37	1.69	1.00	0.06	0.80	2.52	13.02	1.54	2.06	13.51	4.11
3040 m	2.85	2.25	2.11	1.57	0.80	4.56	13.53	2.06	1.22	14.47	3.63
3041	1.29	1.68	0.59	0.19	0.77	2.34	12.65	1.49	1.01	12.99	4.19
3045	1.79	1.71	0.71	0.15	0.76	2.69	12.57	1.65	2.10	13.13	3.79
3051 m	2.95	1.31	2.94	0.68	0.66	4.46	10.85	1.51	2.61	12.11	3.57

was calculated including the corrections made for ozone above the point where the last measurement was performed. For the ACE-FTS, the column between the lowest measurement altitude and the surface was determined using ozone sonde values from that day. Ozone from the ground-based FTSs was retrieved using the 1000 microwindow described in Section 4. A detailed comparison of the FTS instruments, including the ACE-FTS, is presented in a separate paper [34], showing that the Bruker 125HR agrees, with a mean difference of less

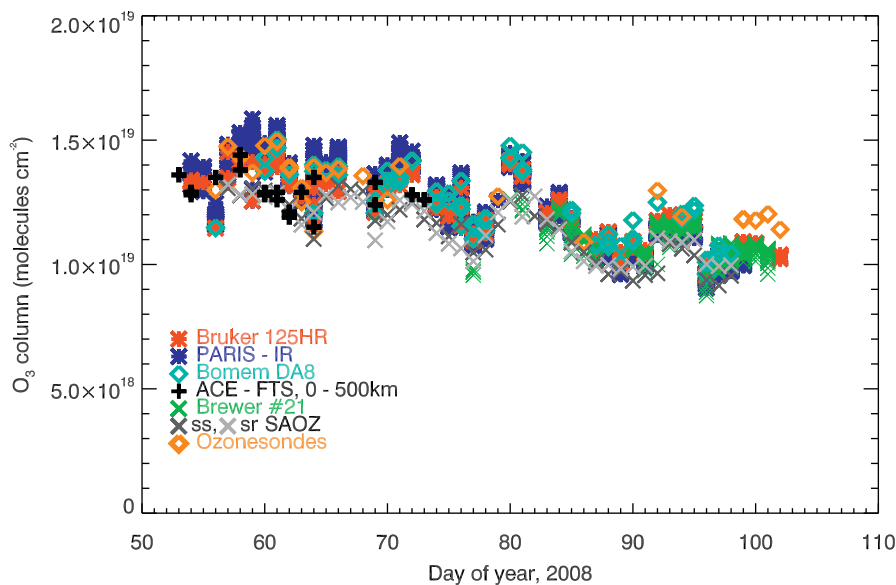
than 2%, with both the DA8 and PARIS FTS and less than 4% with ACE-FTS.

Here, we focus on the comparison between the Bruker 125HR and the two UV–VIS instruments. The correlation and percentage difference plots for the Bruker 125HR versus Brewer #21 are shown in Fig. 7. For this comparison, all direct sun Brewer measurements made within 1 h of each Bruker 125HR spectrum were considered. Good agreement is seen, with both the correlation coefficient and slope close to 1. The mean

Table 6

The error budget for tropospheric ozone partial column (0.6–8 km), for the same spectra as in Table 4.

MW	S _m (%)	S _{temp} (%)	S _{int1} (%)	S _{int2} (%)	S _{sza} (%)	S _{totr} (%)	S _{lint} (%)	S _{width} (%)	S _s (%)	S _{TOTAL} (%)	DOFS
782	16.32	11.83	0.18	1.96	0.36	20.25	6.57	4.08	19.63	29.24	0.61
984	19.08	2.60	7.88	2.25	0.81	20.94	12.01	3.62	22.59	33.26	0.72
984 m	9.99	4.92	0.48	0.38	1.29	11.23	18.76	6.37	21.34	31.21	1.11
987	12.15	2.97	0.09	0.44	1.06	12.56	15.51	6.16	21.19	29.76	1.01
988	17.80	7.25	0.90	0.24	1.34	19.29	19.40	5.70	23.87	36.75	0.94
1000	5.94	5.93	0.12	0.13	0.94	8.46	14.75	5.55	14.76	23.19	1.63
1088	16.86	7.83	0.55	2.28	0.49	18.74	8.14	4.79	14.42	25.46	0.72
1090	13.42	9.97	0.56	1.46	0.53	16.80	7.90	5.11	12.19	22.79	0.87
1106	12.75	12.12	1.37	0.23	0.63	17.66	7.94	6.59	13.53	24.52	0.94
1119	13.95	9.31	0.37	0.73	0.74	16.81	10.77	11.38	16.97	28.56	1.04
1119 m	11.74	8.01	0.47	0.57	0.72	14.25	10.75	10.97	15.49	26.05	1.08
1123	7.25	11.29	0.004	0.11	0.53	13.43	7.82	9.65	14.10	23.10	1.22
1146 m	13.55	19.79	1.31	1.12	0.71	24.06	10.84	6.79	14.52	30.88	1.04
1148	21.77	11.77	1.70	2.37	0.80	24.94	9.68	8.25	21.96	35.58	0.88
1170	24.97	5.65	1.71	0.85	0.42	25.68	7.62	4.94	29.93	40.47	0.55
2775	15.63	3.73	1.05	3.90	0.99	16.60	5.52	9.49	9.97	22.26	0.64
3023	19.13	2.84	5.91	1.42	0.29	20.28	3.16	6.90	36.98	42.85	0.27
3023 m	27.25	5.52	14.34	2.78	0.53	31.41	6.59	12.90	40.63	53.36	0.42
3040 m	21.57	2.45	19.99	18.36	0.14	34.76	1.70	7.49	23.39	42.60	0.16
3041	14.82	4.26	1.46	6.82	0.35	16.93	4.60	10.83	9.35	22.64	0.60
3045	21.76	5.58	5.34	4.30	0.16	23.49	4.45	11.22	32.97	42.24	0.40
3051 m	16.49	2.63	21.02	3.57	0.20	27.08	3.15	3.36	44.35	52.16	0.13

**Fig. 6.** Ozone total columns at Eureka retrieved during spring 2008. All ground-based FTS results used microwindow 1000. The ACE-FTS measurements were acquired within 500 km of PEARL as measured from the ACE-FTS 30 km tangent altitude.

difference is 0.66%, being similar in magnitude to the difference between FTIR and Brewer measurements (1.9%) recorded at Izaña [35]. The differences were calculated with a relation similar to Eq. (3)

$$\%Diff = 100\% \times [(MW1000 - IN)/(MW1000 + IN) * 0.5] \quad (4)$$

where *IN* stands for the instrument in comparison with the Bruker 125HR.

Results of the comparisons with the SAOZ spectrometer are shown in Fig. 8 for sunrise and sunset. For each day, all spectra recorded with the Bruker 125HR before local noon were compared with the sunrise SAOZ measurements, and those recorded after local noon with the sunset SAOZ measurements. The correlation coefficients are again close to 1, with a slightly better correlation for the sunset measurements than the sunrise ones. The mean differences between the instruments for sunset and sunrise are 7.94% and 8.36% respectively,

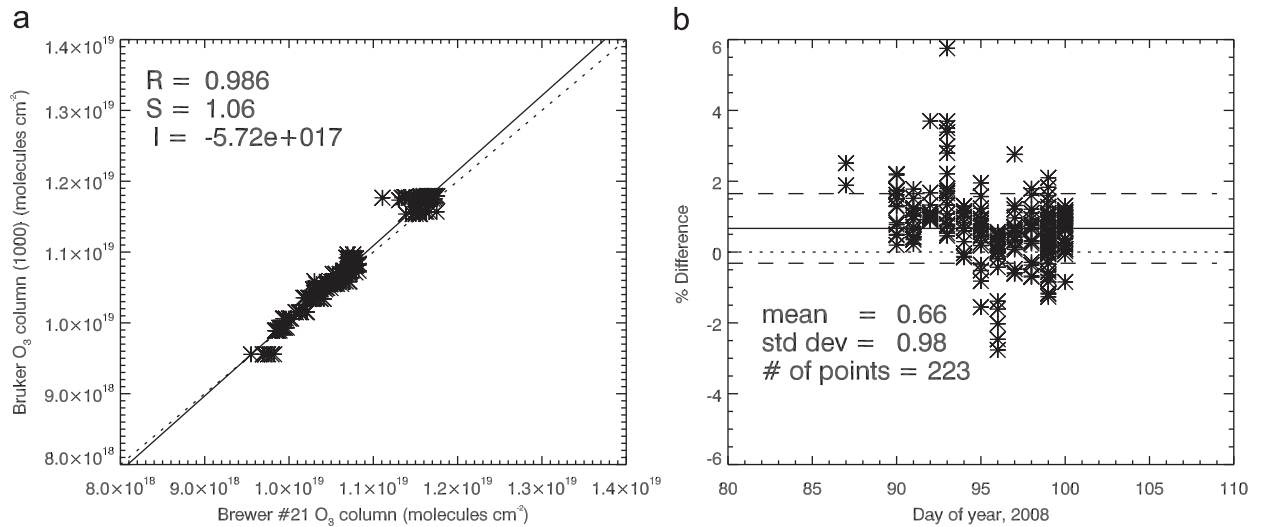


Fig. 7. (a) Scatter plot for ozone total columns retrieved with microwindow 1000 and Brewer #21. The correlation coefficient (R), slope (S) and intercept (I) are given for the comparison. The solid black line shows the best fit for the comparison, and the dotted line shows the 1:1 line. (b) Corresponding percentage differences were calculated using Eq. (4). The mean percentage difference (solid line), standard deviation (dashed lines), and number of points compared are also shown.

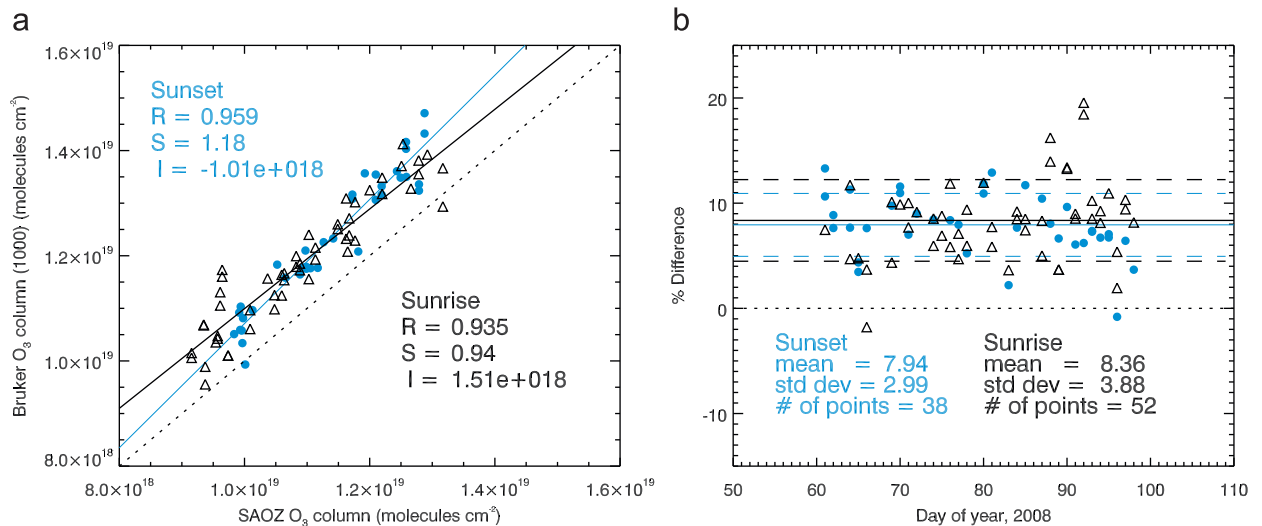


Fig. 8. Same as Fig. 7, but for microwindow 1000 versus SAOZ. Blue represents SAOZ sunset values, gray represents SAOZ sunrise values. (For interpretation of the references to color in this figure legend, the reader is referred to the web version of this article.)

showing that the Bruker 125HR gives higher column values than the SAOZ spectrometer (similar to differences of 4–7% shown in [36]). This offset is clearly seen in Fig. 6, and is most likely related to the very different observing geometry of the two instruments. SAOZ views scattered sunlight from the twilight zenith-sky, while the Bruker 125HR is solar pointing, with an atmospheric path that can extend hundreds of kilometers in the direction of the sun.

Total ozone columns are obtained by integrating the ozone sonde profiles from ground level to the maximum height reached by the sonde and correcting for the atmosphere above. Ozone sondes are launched daily during the

spring campaigns and once a week throughout the rest of the year. For the 2008 campaign, ozone sonde columns are compared with the Bruker 125HR in Fig. 9. The correlation coefficient for this comparison is 0.941, the slope is 1.16 and the intercept is of order 10¹⁸ molec/cm². The mean difference in column of -6.94% indicates that the sonde columns are larger than the columns obtained with the 1000 microwindow, while the standard deviation (4.23%) indicates some scatter in the column differences (similar comparisons were done in [35] and [17]). These results may again be related to the different air masses being sampled by the two instruments, as the Arctic stratosphere is highly variable in time and space at this time of the year.

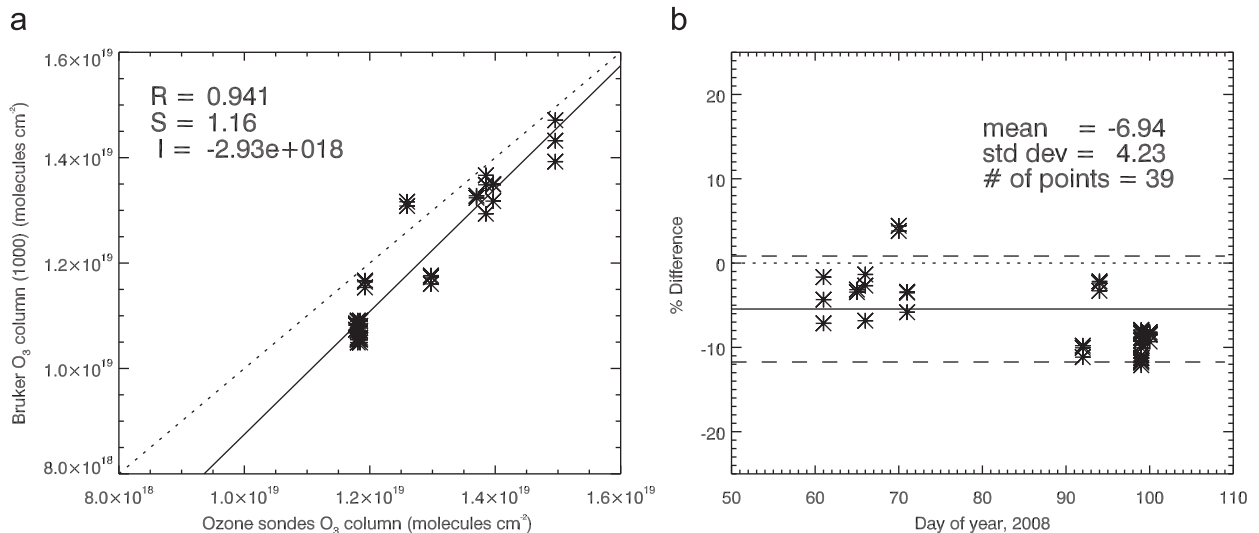


Fig. 9. Same as Fig. 7, but for microwindow 1000 versus ozone sondes.

6. Conclusions

The purpose of this study was to optimize the ozone retrievals for mid-infrared FTIR measurements made with the Bruker 125HR at Eureka. In particular, the choice of retrieval microwindow(s) has been investigated by examining 22 different spectral regions. Averaging kernels, DOFS, and error budgets were determined for each microwindow, using both spring and summer spectra. The filter 6 region (600–1400 cm⁻¹) shows more sensitivity in both the stratosphere and troposphere than the filter 3 region (2400–3100 cm⁻¹), with a somewhat smaller total error and higher DOFS. Microwindow 1000 (1000–1004.5 cm⁻¹) was shown to have the highest sensitivity to both the stratosphere and troposphere. The quantity of information given by this microwindow is very high, with close to 7 DOFS for the total column, and more than 1.5 DOFS for the tropospheric partial column. The total error is one-third to one-half of the total error found for the other microwindows for the total column. These results support the choice of this microwindow for the evaluation of tropospheric and stratospheric ozone trends over Western Europe performed by the European ground-based FTIR network UFTIR (Upper Free Troposphere observations from a European ground-based FTIR network) [37] and by [38,44,18], and [17] from Table 1.

Ozone measurements retrieved using the 1000 microwindow were compared with several other instruments at Eureka during the spring 2008 Canadian Arctic ACE validation campaign. These comparisons showed mean agreement of approximately 2% with the two additional ground-based FTs, 4% with the satellite-based ACE-FTS, 0.7% with the Brewer spectrophotometer, 8% with the SAOZ spectrometer, and 7% with the ozone sondes. The higher differences for the latter two comparisons are likely indicative of the different air masses being sampled by these instruments.

Acknowledgments

The authors wish to thank the staff at the Eureka weather station and CANDAC for the logistical and on-site support provided at Eureka. They also thank CANDAC/PEARL Principal Investigator James R. Drummond, PEARL Operations Manager Pierre Fogal, and Ashley Harrett, Alexei Khmel, Paul Loewen, Keith MacQuarrie, Oleg Mikhailov, and Matt Okraszewski, the CANDAC operators, for their invaluable assistance in maintaining the instrument and taking measurements. CANDAC and PEARL are funded by the Atlantic Innovation Fund/ Nova Scotia Research Innovation Trust, Canadian Foundation for Climate and Atmospheric Sciences, Canadian Foundation for Innovation, Canadian Space Agency (CSA), Environment Canada, Government of Canada International Polar Year funding, Natural Sciences and Engineering Research Council (NSERC), Ontario Innovation Trust, Polar Continental Shelf Program and the Ontario Research Fund.

The Atmospheric Chemistry Experiment, onboard SCISAT, is a Canadian-led mission mainly supported by the CSA and NSERC. The Canadian Arctic ACE validation campaigns are supported by the CSA, Environment Canada, NSERC, and the Northern Scientific Training Program.

The SAOZ participation in the campaign was supported by the Centre National d'Études Spatiales. The daily ozone sondes were launched by Environment Canada personnel.

References

- [1] Schonbein CF. On the odour accompanying electricity and on the probability of its dependence on the presence of a new substance. *Philos Mag (III)* 1840;17:293–4.
- [2] Schonbein CF. Recherche sur la nature de l'odeur, qui se manifeste dans certaines actions chimiques. *C R Hebd Seances Acad Sci C* 1840;10:706–10.

- [3] Fabry C. L'ozone atmosferique. Paris, France: Centre Nationale de la Recherche Scientifique; 1950.
- [4] Fabry C, Buisson H. L'absorption de l'ultraviolet par l'ozone et la limite du spectre solaire. *J Phys Rad* 1913;5:196–206.
- [5] Bronnimann S, Staehelin J, Farmer SFG, Cain JC, Swendby T, Svenoe T. Total ozone observations prior to the IGY I: a history. *Q J R Meteorol Soc* 2003;129:2797–817.
- [6] Dobson GMB, Harrison DN. Observations of the amount of ozone in the Earth's atmosphere and its relation to other geophysical conditions. *Proc R Soc London* 1926;A110:660–93.
- [7] Kerr JB, McElroy CT, Olafson RA. Measurements of ozone with the Brewer spectrophotometer. In: Proceedings of the quadrennial international ozone symposium. Boulder, CO; 1981. p. 74–9.
- [8] Murcray DG, Murcray FH, Williams WJ, Kyle TG, Goldman A. Variation of the infrared solar spectrum between 700 cm⁻¹ and 2240 cm⁻¹ with altitude. *Appl Opt* 1969;8:2519–36.
- [9] Farmer CB. Infrared measurements of stratospheric composition. *Can J Chem* 1974;52:1544–59.
- [10] Bell RJ. Introductory Fourier transform spectroscopy. New York: Academic Press; 1972.
- [11] Kurylo MJ, Zander R. The NDSC-its status after 10 years of operation. In: Proceedings of the XIX quadrennial ozone symposium. Hokkaido University Sapporo; Japan; July 3–8, 2000. p. 167–8; Kurylo MJ. 10 years of the network for the detection of stratospheric change. In: NDSC symposium. Arcachon, France; September 24–27, 2001.
- [12] Rodgers CD. Retrieval of atmospheric temperature and composition from remote measurements of thermal radiation. *Rev Geophys* 1976;14(4):609–24.
- [13] Rodgers CD. Characterization and error analysis of profiles retrieved from remote sounding measurements. *J Geophys Res* 1990;95:5587–5595.
- [14] Rodgers CD. Inverse methods for atmospheric sounding: theory and practice. Series on atmospheric, oceanic and planetary physics, vol. 2. New Jersey: World Scientific Publishing Co Pte Ltd; 2000.
- [15] Pougatchev NS, Connor BJ, Rinsland CP. Infrared measurements of the ozone vertical distribution above Kitt Peak. *J Geophys Res* 1995;100:16689–97.
- [16] Hamdouni A, Barbe A, Demoulin P, Zander R. Retrieval of ozone vertical column amounts from ground-based high resolution infrared solar spectra. *JQSRT* 1997;57:11–22.
- [17] Barret B, De Mazière M, Demoulin P. Retrieval and characterization of ozone profiles from solar infrared spectra at the Jungfraujoch. *J Geophys Res* 2002 doi:10.1029/2001JD001298.
- [18] Schneider M, Hase F. Technical note: recipe for monitoring of total ozone with a precision of around 1DU applying mid-infrared solar absorption spectra. *Atmos Chem Phys* 2008;8:63–71.
- [19] Batchelor RL, Strong K, Lindenmaier R, Mittermeier RL, Fast H, Drummond JR, Fogal PF. A new Bruker IFS 125HR FTIR spectrometer for the Polar Environment Atmospheric Research Laboratory at Eureka, Canada—measurements and comparison with the existing Bomem DA8 spectrometer. *J Atmos Oceanic Technol* 2009;26(7) doi:10.1175/2009JTECHA12151.
- [20] Pougatchev NS, Connor BJ, Jones NB, Rinsland CP. Validation of ozone profile retrievals from infrared ground-based solar spectra. *Geophys Res Lett* 1996;23:1637–40.
- [21] Rinsland CP, Goldman A, Murcray FJ, Murcray FH, Blatherwick RD, Murcray DG. Infrared measurements of atmospheric gases above Mauna Loa, Hawaii, in February 1987. *J Geophys Res* 1988;93:12607–12626.
- [22] Meier A, Goldman A, Manning PS, Stephen TM, Rinsland CP, Johnes, NB, et al. Improvements to air mass calculations for ground-based infrared measurements. *JQSRT* 2004;83:109–13.
- [23] Brühl C, Drayson SR, Russell III JM, McInerney JM, Purcell PN, Claude, H, et al. Halogen Occultation Experiment ozone channel validation. *J Geophys Res* 1996;101:10217–40.
- [24] Rothman LS, Jacquemart D, Barbe A, Benner DC, Birk M, Brown, LR, et al. The HITRAN 2004 molecular spectroscopic database. *JQSRT* 2005;96:139–204.
- [25] Rodgers CD, Connor BJ. Intercomparison of remote sounding instruments. *J Geophys Res* 2003 doi:10.1029/2002JD002299.
- [26] Mondelain D, Payan S, Deng W, Camy-Peyret C, Hurtmans D, Mantz AW. Measurements of the temperature dependence of line mixing and pressure broadening parameters between 296 and 90K in the ν_3 band of ¹²CH₄ and their influence on atmospheric methane retrievals. *J Mol Spectrosc* 2007;244:130–7.
- [27] Kerzenmacher TE, Walker KA, Strong K, Berman R, Bernath PF, Boone, CD, et al. Measurements of O₃, NO₂ and temperature during the 2004 Canadian Arctic ACE validation campaign. *Geophys Res Lett* 2005 doi:10.1029/2005GL023032.
- [28] Fu D, Walker KA, Mittermeier RL, Strong K, Sung K, Fast, H, et al. Simultaneous atmospheric measurements using two Fourier transform infrared spectrometers at the Polar Environment Atmospheric Research Laboratory during spring 2006, and comparisons with the Atmospheric Chemistry Experiment—Fourier Transform Spectrometer. *Atmos Chem Phys Discuss* 2008;8:5305–5358.
- [29] Farahani EE, Fast H, Mittermeier RL, Makino Y, Strong K, McLandress, C, et al. Nitric acid measurements at Eureka obtained in winter 2001–2002 using solar and lunar Fourier transform absorption spectroscopy: comparisons with observations at Thule and Kiruna and with results from three-dimensional models. *J Geophys Res* 2007 doi:10.1029/2006JD00709605.
- [30] Fu D, Walker KA, Sung K, Boone CD, Soucy MA, Bernath PF. The portable atmospheric research interferometric spectrometer for the infrared, PARIS-IR. *JQSRT* 2007;103:362–70.
- [31] Savastiouk V, McElroy CT. Brewer spectrophotometer total ozone measurements made during the 1998 middle atmosphere nitrogen trend assessment (MANTRA) campaign. *Atmos Ocean* 2005;43(4):315–324.
- [32] Pommereau JP, Goutail F. O₃ and NO₂ ground based measurements by visible spectrometry during Arctic winter and spring 1988. *Geophys Res Lett* 1988;15:891–4.
- [33] Bernath PF, McElroy CT, Abrams MC, Boone CD, Butler M, Camy-Peyret, C, et al. Atmospheric Chemistry Experiment (ACE): mission overview. *Geophys Res Lett* 2005 doi:10.1029/2005GL022386.
- [34] Batchelor RL, Kolonjari F, Lindenmaier R, Mittermeier RL, Daffer W, Fast H, Manney G, Strong K, Walker KA. Four Fourier transform spectrometers and the Arctic polar vortex: Instrument intercomparison and ACE-FTS validation at Eureka during the IPY springs of 2007 and 2008. *Atmos Meas Tech Discuss* 2009;2:1–37.
- [35] Schneider M, Blumenstock T, Hase F, Höpfner M, Cuevas E, Redondas A, Sancho JM. Ozone profiles and total column amounts derived at Izaña, Tenerife Island, from FTIR solar absorption spectra, and its validation by an intercomparison to ECC-sonde and Brewer spectrometer measurements. *JQSRT* 2005;91:245–74.
- [36] Fraser A, Bernath PF, Blatherwick RD, Drummond JR, Fogal PF, Fu D, Goutail, F, et al. Intercomparison of ground-based ozone and NO₂ measurements during the MANTRA 2004 campaign. *Atmos Chem Phys* 2007;7:5489–99.
- [37] Vigouroux C, De Mazière M, Demoulin P, Servais C, Hase F, Blumenstock, T, et al. Evaluation of tropospheric and stratospheric ozone trends over Western Europe from ground-based FTIR network observations. *Atmos Chem Phys* 2008;8:6865–86.
- [38] Senten C, De Mazière M, Dils B, Hermans C, Kruglanski M, Neefs, E, et al. Technical note: new ground-based FTIR measurements at Ile de La Réunion: observations, error analysis, and comparisons with independent data. *Atmos Chem Phys* 2008;8:3483–508.
- [39] Wunch D, Taylor JR, Fu D, Bernath P, Drummond JR, Midwinter C, Strong K, Walker KA. Simultaneous ground-based observations of O₃, HCl, N₂O, and CH₄ over Toronto, Canada by three Fourier transform spectrometers with different resolutions. *Atmos Chem Phys* 2007;7:1275–92.
- [40] Taylor JR, Wunch D, Midwinter C, Wiacek A, Drummond JR, Strong K. An extended intercomparison of simultaneous ground-based Fourier transform infrared spectrometer measurements at the Toronto Atmospheric Observatory. *JQSRT* 2008;109:2244–60.
- [41] Yamamori M, Kagawa A, Kasai Y, Mizutani K, Murayama Y, Sugita T, Irie H, Nakajima H. Validation of ILAS-II version 1.4 O₃, HNO₃, and temperature data through comparison with ozonesonde, ground-based FTS, and lidar measurements in Alaska. *J Geophys Res* 2006 doi:10.1029/2005JD006438.
- [42] Kagawa A, Kasai Y, Jones NB, Yamamori M, Seki K, Murcray F, Murayama Y, Mizutani K, Itabe T. Characteristics and error estimation of stratospheric ozone and ozone-related species over Poker Flat (65°N, 147°W), Alaska observed by a ground-based FTIR spectrometer from 2001 to 2003. *Atmos Chem Phys* 2007;7:3791–3810.
- [43] Sung K, Skelton R, Walker KA, Boone CD, Fu D, Bernath P. N₂O and O₃ Arctic column amounts from PARIS-IR observations: retrievals, characterization and error analysis. *JQSRT* 2007;107:385–406.
- [44] Griesfeller A, Griesfeller J, Hase F, Kramer I, Loës P, Mikuteit, S, et al. Comparison of ILAS-II and ground-based FTIR measurements of O₃, HNO₃, N₂O, and CH₄ over Kiruna, Sweden. *J Geophys Res* 2006;111(D11S07) doi:10.1029/2005JD006451.
- [45] Hase F, Hannigan JW, Coffey MT, Goldman A, Höpfner M, Jones NB, Rinsland CP, Wood SW. Intercomparison of retrieval codes used for

- the analysis of high-resolution, ground-based FTIR measurements. *JQSRT* 2004;87:25–52.
- [46] Meier A, Paton-Walsh C, Bell W, Blumenstock T, Hase F, Goldman, A, et al. Evidence of reduced measurement uncertainties from an FTIR instrument intercomparison at Kiruna, Sweden. *JQSRT* 2005; 96:75–84.
- [47] Notholt J, Toon GC, Rinsland CP, Pougatchev NS, Jones NB, Connor, BJ, et al. Latitudinal variations of trace gas concentrations in the free troposphere measured by solar absorption spectroscopy during a ship cruise. *J Geophys Res* 2000;105:1337–49.
- [48] Goldman A, Paton-Walsh C, Bell W, Toon GC, Blavier JF, Sen, B, et al. Network for the Detection of Stratospheric Change Fourier transform infrared intercomparison at Table Mountain Facility, November 1996. *J Geophys Res* 1999;104:30481–503.
- [49] Rinsland CP, Connor BJ, Jones NB, Boyd I, Matthews WA, Goldman, A, et al. Comparison of infrared and Dobson total ozone columns measured from Lauder, New Zealand. *Geophys Res Lett* 1996; 23:1025–8.
- [50] Adrian GP, Blumenstock T, Fischer H, Gerhardt L, Gulde T, Oelhaf H, et al. Column amounts of trace gases derived from ground-based measurements with MIPAS during CHEOPS III. *Geophys Res Lett* 1991;18:783–6.
- [51] Wegner A, Stiller GP, Von Clarmann T, Maucher G, Blumenstock T, Thomas P. Sequestration of HNO_3 in polar stratospheric clouds and chlorine activation as monitored by ground-based Fourier transform infrared solar absorption measurements. *J Geophys Res* 1998; 103:22181–200.